Acidic pH retards the fibrillization of human islet amyloid polypeptide due to electrostatic repulsion of histidines

Yang Li, Weixin Xu, Yuguang Mu, and John Z. H. Zhang

Citation: J. Chem. Phys. **139**, 055102 (2013); doi: 10.1063/1.4817000
View online: http://dx.doi.org/10.1063/1.4817000
View Table of Contents: http://jcp.aip.org/resource/1/JCPSA6/v139/i5
Published by the AIP Publishing LLC.

Acidic pH retards the fibrillization of human islet amyloid polypeptide due to electrostatic repulsion of histidines

Yang Li,[1,2] Weixin Xu,[1,2,a)] Yuguang Mu,[3] and John Z. H. Zhang[1,2,4,a)]
[1]*State Key Laboratory of Precision Spectroscopy, Department of Physics, East China Normal University, Shanghai 200062, China*
[2]*Institute of Theoretical and Computational Science, Institutes for Advanced Interdisciplinary Research, East China Normal University, Shanghai 200062, China*
[3]*School of Biological Sciences, Nanyang Technological University, Singapore*
[4]*Department of Chemistry, New York University, New York, New York 10003, USA*

(Received 12 May 2013; accepted 15 July 2013; published online 1 August 2013)

The human Islet Amyloid Polypeptide (hIAPP) is the major constituent of amyloid deposits in pancreatic islets of type-II diabetes. IAPP is secreted together with insulin from the acidic secretory granules at a low pH of approximately 5.5 to the extracellular environment at a neutral pH. The increased accumulation of extracellular hIAPP in diabetes indicates that changes in pH may promote amyloid formation. To gain insights and underlying mechanisms of the pH effect on hIAPP fibrillogenesis, all-atom molecular dynamics simulations in explicit solvent model were performed to study the structural properties of five hIAPP protofibrillar oligomers, under acidic and neutral pH, respectively. In consistent with experimental findings, simulation results show that acidic pH is not conducive to the structural stability of these oligomers. This provides a direct evidence for a recent experiment [L. Khemtemourian, E. Domenech, J. P. F. Doux, M. C. Koorengevel, and J. A. Killian, J. Am. Chem. Soc. **133**, 15598 (2011)], which suggests that acidic pH inhibits the fibril formation of hIAPP. In addition, a complementary coarse-grained simulation shows the repulsive electrostatic interactions among charged His18 residues slow down the dimerization process of hIAPP by twofold. Besides, our all-atom simulations reveal acidic pH mainly affects the local structure around residue His18 by destroying the surrounding hydrogen-bonding network, due to the repulsive interactions between protonated interchain His18 residues at acidic pH. It is also disclosed that the local interactions nearby His18 operating between adjacent β-strands trigger the structural transition, which gives hints to the experimental findings that the rate of hIAPP fibril formation and the morphologies of the fibrillar structures are strongly pH-dependent. © *2013 AIP Publishing LLC*. [http://dx.doi.org/10.1063/1.4817000]

I. INTRODUCTION

It is well known that amyloid fibrils formed by amyloidogenic proteins/peptides, such as amyloid-β peptide, α-synuclein, and human Islet Amyloid Polypeptide (hIAPP), are linked to several neurodegenerative diseases including Alzheimer's, prion diseases and type-II diabetes mellitus (T2DM).[1–3] Among these neurodegenerative diseases, T2DM affects millions of people worldwide, which is characterized by chronic insulin resistance and progressive decline in pancreatic β-cell function.[4,5] One of the most common pathological features of T2DM is the presence of fibrillar amyloid deposits in the islets of Langerhans of the pancreas.[6–9] Once amounts of toxic amyloid aggregates occur, β cells are damaged, and it may induce the dysfunction of islet cell and death in T2DM eventually.[10–12]

The 37-residue hIAPP, also known as amylin is the major constituent of amyloid deposits in pancreatic islets of T2DM.[13,14] Amyloid fibrils of hIAPP fibrils are self-assembled, β-sheet-rich aggregates that typically exhibit diameters in the 5-15 nm range and lengths in the 0.1–10 nm range.[15–17] The fibrils are made up of hIAPP β-strands running perpendicular to the fibril axis, 4.7 Å apart, and are linked by hydrogen bonds that run approximately parallel to the long axis. The monomeric subunit consists of two β-strands connected by a turn, thus forming a U-shaped topology. Amyloid growth can proceed longitudinally (i.e., the adsorption of new monomers along the fibril axis) and laterally (i.e., the interactions with another stack of monomers at the lateral surface of the growing fiber).[18–20] The monomeric hIAPP has a Cys2-Cys7 disulfide bridge, an amidated C terminus,[13,14] and a single His residue at position 18 whose protonation state is affected by the pH change from intragranular to extracellular environments.

Up to now, it is known that some factors, such as agitation,[21] ionic strength,[22] metal ions,[23] surface,[24,25] small molecules,[26] amino acid substitutions at various positions,[27,28] template,[29] and protein components such as insulin,[30] proinsulin, and proIAPP, may affect the formation/stability of amyloid fibrils. Islet Amyloid Polypeptide (IAPP) is stored in the β-cell granules of the pancreas at a pH of approximately 5.5 and released into the extracellular space at a pH of 7.4.[31] HIAPP is cosecreted with insulin into the circulation as a soluble monomer,[32–34] and amyloid

a)Authors to whom correspondence should be addressed. Electronic mail: wxxu@sat.ecnu.edu.cn and john.zhang@nyu.edu

is formed in pancreatic islets in the extracellular department which are at neutral pH. Thus, pH may be one of many factors keeping IAPP from misfolding into amyloid fibrills. Recently, the experimental work by Khemtemourian *et al.*[35] found that an acidic pH (5.5) prevents aggregation and membrane damage of hIAPP in the secretory granules. And previously, it was also found that the morphologies of the fibrillar structures and the aggregation of hIAPP are highly sensitive to pH values.[35–37] Nevertheless, the underlying microscopic inhibition mechanisms of acidic pH to hIAPP aggregation and resulting cytotoxicity is still unknown. Here, we use computer simulations to gain insights into the mechanism of the effects of pH on the structure and stability of the hIAPP protofibrillar oligomer since it is the highly toxic form to β cells.

In this study, we carried out a series of all-atom MD simulations at room temperature using the standard AMBER99SB force field[38] at pH 5.5 and 7.4, respectively. The structures we used consist of one to five full-length hIAPP protofibrillar subunits, each of which consists of two antiparallel β-sheet layers. In consistent with experimental findings,[35] simulation results show that acidic pH is not conducive to the structural stability of the hIAPP protofibrillar oligomers. Monomeric hIAPP contains one His18 residue, whose charge state depends on pH: protonated at pH 5.5 and deprotonated at pH 7.4. We have carefully compared two kinds of structures at pH 5.5 and 7.4 and found that His18 is possibly responsible for the pH-dependent behavior of hIAPP aggregation. In an effort to explain the microscopic origin of this pH dependence, we conducted a series of analysis on the local structure around residue His18. It is found that acidic pH mainly affects the local structure around residue His18 by destroying the local hydrogen-bonding network, due to the repulsive electrostatic interactions between charged interchain His18 residues. Consequently, the ionization state of His18 modulated by pH environment influences the stability of hIAPP protofibrillar oligomers, and possibly the morphologies of the mature fibrillar structures.

II. MODEL AND METHODS

A. All-atom simulation setup and protocol

To mimic the environment of the two pH values, the side chains of all the His18 residues were modeled to take different charge states: positively charged at pH 5.5 and neutral at pH 7.4. The same strategy is often applied in MD simulations to investigate the pH-dependent behaviors of protein folding/aggregation.[39–41] In such a way, the pH condition is accounted for by choosing the charge state of His18 in our simulations.

In our simulations, the initial hIAPP protofibrillar structure is provided by the Eisenberg group.[17] The structure consists of one to five subunits, each of which contains two antiparallel β-sheet layers of full-length hIAPP (see the five-subunits system as an example in Figure 1(a)). For simplicity, we use the following nomenclature for the five hIAPP oligomeric species: AFS1 (one subunit), AFS2 (two subunits), AFS3 (three subunits), AFS4 (four subunits), AFS5 (five subunits), respectively. In one subunit,

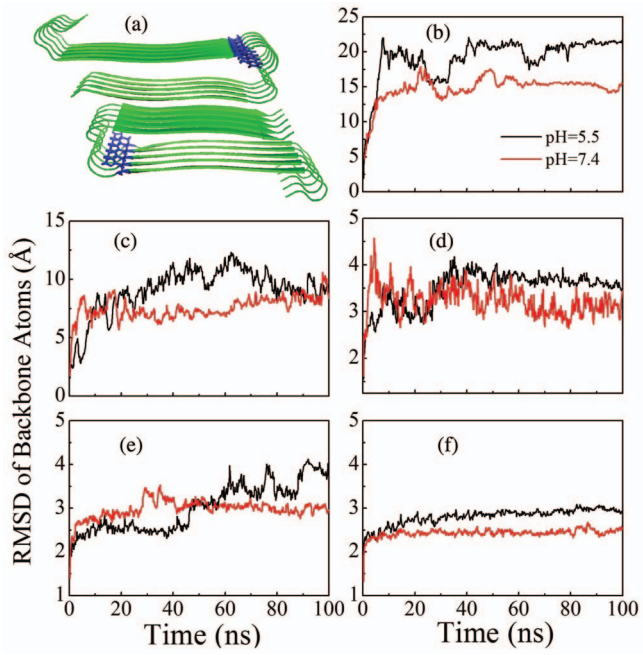

FIG. 1. (a) Initial structure of the hIAPP protofibril that consists of two antiparallel β-sheet layers, with each layer containing 5 full-length hIAPP monomers. (b)–(f) Backbone RMSD values of the hIAPP protofibrillar oligomers AFS1, AFS2, AFS3, AFS4, and AFS5, respectively, as a function of simulation time for pH 5.5 (black curves) and 7.4 (red curves) at 300 K.

the interface of two β-sheet layers is in a steric zipper pattern formed by side chains. The sequence of the full-length hIAPP is KCNTATCATQRLANFLVHSSNNFGAILSSTNVGSNTY. Each β-sheet layer is arranged in a β-strand-turn-β-strand/U fold, including an N-terminal β-strand (residues 6-18), a turn (residues 19-24) and a C-terminal β-strand (residues 25-36). In order to study the effect of pH on the structure and stability of hIAPP protofibrillar oligomers, several 100-ns MD simulations were performed using GROMACS software package,[42] under AMBER99SB force field[43] at T = 300 K with pH 5.5 and 7.4, respectively. Each system was solvated with explicit TIP3P water molecules in a cubic box of size more than 90 Å. Periodic boundary conditions (PBC) are used in MD simulations to minimize the problems with boundary effects caused by finite size. To neutralize the simulation system, 4 chloride ions and 3 chloride ions were added to each hIAPP peptide at pH 5.5 and 7.4, respectively. As an example, 30 chloride ions were added for AFS5 at pH 7.4. Following energy minimization using the steepest descent, two 100-ps equilibrations were separately conducted under NVT ensemble and NPT ensemble to arrive at the correct temperature and reach the proper density. In the production run, the NPT ensemble was used. The protein and water groups were separately coupled to an external heat bath with a relaxation time of 0.1 ps. The modified Berendsen thermostat of V-rescale and Parrinello-Rahman manostat were applied, which can generate a proper ensemble. All bonds involving hydrogen atoms were constrained in length according to LINCS protocol.[44] A time step of 2 fs was used and the trajectories were output every 2 ps. Previous simulation work has demonstrated that, in comparison with the cases where the electrostatic interactions are truncated even with a large

truncation distance of 25 Å, the simulation results obtained using the particle mesh Ewald (PME) method are more consistent with experiments.[45] For electrostatic interactions, we thus used the PME method[46] with a 10 Å cutoff; for van der Waals interactions, we set the cutoff as 12 Å.

B. Structure-based coarse-grained model

In order to test the effect of ionization state of His18 on hIAPP aggregation, a structure-based coarse-grained model[47–50] is applied to simulate the dimerization of two full-length hIAPP monomers with the His18 residues in non-charged or charged states. Proteins are coarse-grained in a C_α level of simplification and the Hamiltonian that gives the interaction energy is structure based. Proteins are modeled with residues represented as single beads located at the C_α atoms positions. The potential V of hIAPP dimer is given as

$$\begin{aligned} V &= V_{\text{bonded}} + V_{\text{bond-angle}} + V_{\text{dihedral}} + V_{\text{non-bonded}} \\ &= \sum_{\text{bonds}}^{N-1} K_r(r - r_0)^2 + \sum_{\text{bond-angles}}^{N-2} K_\theta(\theta - \theta_0) \\ &\quad + \sum_{\text{dihedrals}}^{N-3} \left\{ K_\phi^{(1)}[1 - \cos(\phi - \phi_0)] \right. \\ &\quad \left. + K_\phi^{(3)}[1 - \cos 3(\phi - \phi_0)] \right\} \\ &\quad + \sum_{i<j-3}^{\text{native}} \epsilon \left[5\left(\frac{\sigma_{ij}}{r_{ij}}\right)^{12} - 6\left(\frac{\sigma_{ij}}{r_{ij}}\right)^{10} \right] \\ &\quad + \sum_{i<j-3,else}^{\text{non-native}} \epsilon \left(\frac{\sigma_0}{r_{ij}}\right)^{12} \\ &\quad + \sum_{i,j}^{\text{electrostatic}} \left(\frac{q_i q_j}{4\pi\varepsilon_0\varepsilon_r r_{ij}}\right) e^{-r/l_D}. \end{aligned} \tag{1}$$

Here, r, θ, and ϕ represent the virtual bond length, bond-angle, and dihedral angle, respectively, r_{ij} is the spatial distance between the ith and the jth residues and σ_{ij} is their distance in the native conformation. Here the dimer structure extracted from the experimental hIAPP protofibril is taken as the native conformer. r_0, θ_0, and ϕ_0 correspond to the values extracted from the native coordinates of a conformer. For more details about the parameters please refer to the literature.[49,50] In this equation, adjacent beads interact via harmonic interactions. Angles formed by monomer i, $i+1$, and $i+2$ are also maintained by a harmonic potential energy function. Dihedral angles formed by 4 adjacent residues are given cosine potential energy functions. The native contact pairs of residues are assigned as an attractive interaction of a 10–12 Lennard-Jones (LJ) potential. All residue pairs which are not in contact in the native conformer, interact via non-specific repulsion to prevent chain crossing. Here, two residues are defined as a "native contact" if the distance between any pair of non-hydrogen atoms belonging to these two residues, respectively, is shorter than 7 Å in the native conformation. The fraction of native contacts Q, of a given structure during a simulation at a time t is defined as the fraction of number of native contacts present on the current structure at t over the total number of native contacts present on the native conformer. In our simulations, the initial structure of hIAPP dimer is obtained from the unfolded ensemble after a long-time high-temperature (500 K) unfolding simulation using the above coarse-grained model, of which two monomers are in random coil conformations (shown in Fig. 8). Then two comparative simulations at T = 300 K were performed.

C. Analysis methods

The Dictionary of Secondary Structure of Proteins (DSSP) algorithm written by Kabsch and Sander[51] was used to identify secondary structure conformation of the hIAPP protofibrillar oligomers.

The conformational entropy can provide valuable information about the flexibility of a given conformer.[40,52] Performing a full vibrational analysis, the intrinsic entropy characteristics of helix formation and the stability of other secondary structures were successfully investigated recently.[53] Here, the absolute entropy is estimated by the quasiharmonic analysis or the essential dynamics method.[54] The covariance matrix is constructed as

$$\sigma_{ij} = \langle (x_i - \langle x_i \rangle)(x_j - \langle x_j \rangle) \rangle, \tag{2}$$

where $x_i \ldots x_{3N}$ are the mass-weighted Cartesian coordinates of the N-particle system and $\langle \ldots \rangle$ denotes the average over all sampled conformations. Hence, the covariance matrix provides information on the correlated fluctuations of pairs of atoms. The eigenvectors and eigenvalues λ_i of σ yield the modes of collective motion and their amplitudes. Based on the quasiharmonic approximation the configuration entropy is given by

$$S = k_B \sum_{i}^{3n-6} \frac{\hbar\omega_i / k_B T}{e^{\hbar\omega_i / k_B T} - 1} \log(1 - e^{-\hbar\omega_i / k_B T}), \tag{3}$$

where $\omega_i = \sqrt{(k_B T / \lambda_i)}$, k_B, $\hbar$, and T are the Boltzmann constant, reduced Planck constant, and the temperature, respectively.

III. RESULTS AND DISCUSSION

A. Full system

1. Conformational drift

First, we explored the conformational dynamics of the hIAPP protofibrillar oligomers AFS1, AFS2, AFS3, AFS4, and AFS5, respectively. For these systems, we performed two kinds of simulations under both pH 5.5 and 7.4. The overall extent of conformational drift with respect to the initial structure is measured by root-mean-square deviation (RMSD) of backbone atoms in each simulation (Figures 1(b)–1(f)). The comparison clearly shows that the overall stability of the hIAPP protofibrillar assembly in solution environment is quite different at two pH values. The RMSD of AFS5 (Figure 1(f)) at pH 7.4 is relatively smaller than that at pH 5.5, indicating a smaller conformational drift. From other curves

shown in Figures 1(b)–1(e), it is noticed that other hIAPP protofibril species at pH 7.4 also have relatively smaller RMSD than those at pH 5.5, and the values stay relatively stable throughout the simulation time. For example, the RMSD of AFS4 (Figure 1(e)) fluctuates around 3 Å at pH 7.4, while the AFS4 at pH 5.5 shows a larger fluctuating RMSD that reaches as high as 4 Å in the 100-ns simulation. In general, it is clearly shown that the hIAPP protofibrillar oligomer under low pH value (5.5) is more flexible, which indicates that low pH destabilizes the assembly structure. It is noted that the RMSD values of AFS1 (Figure 1(b)) is exceptionally large (up to 20 Å). The dimeric structure is found to be severely distorted (data not shown), which indicates that the dimer conformer of hIAPP may be unstable in solution environment. In addition, it is noticed that the RMSD values decrease with the growth of the hIAPP protofibrillar size from AFS1 to AFS5. This suggests that the bigger the nuclear-like assembly is, the more stable the structure becomes. This is consistent with the nuclear-dependent mechanism of amyloid fribrillization.

2. Hydrogen-bonding network

The structural framework of hIAPP amyloid aggregates is mainly stabilized by a rich backbone hydrogen-bonding (H-bond) network. It is thus expected that there are some differences in the H-bond number of the hIAPP protofibrillar oligomers at pH 5.5 and 7.4. So we calculated the H-bond number for AFS1, AFS2, AFS3, AFS4, and AFS5, respectively. The average H-bond number of the last 30-ns trajectory for each simulation is shown as histograms in Figure 2. The green histogram is for pH 5.5, while the red one is for 7.4. Here the formation of a hydrogen bond is defined if the distance between two heavy atoms (N and O in this case) is less than 3.5 Å and the angle N–H–O is larger than 120°. As expected, from the comparison of H-bond histograms in Figure 2, oligomers under neutral (7.4) and acidic conditions (5.5) show different H-bond networks. Obviously, the distribution based on simulations at pH 7.4 is composed preferentially of high occupancy of H-bond number. In contrast, the distribution based on simulations at pH 5.5 shows a low occupancy of H-bond number. As an example, the average H-bond number of AFS5 reaches 311 at pH 7.4, while it is 302 at pH 5.5. In a word, the hIAPP oligomers at pH 7.4 possess more hydrogen bonds than those at pH 5.5. Thus, low pH somehow destroys the H-bond network somewhere in the hIAPP oligomers, which will be further explored in the following.

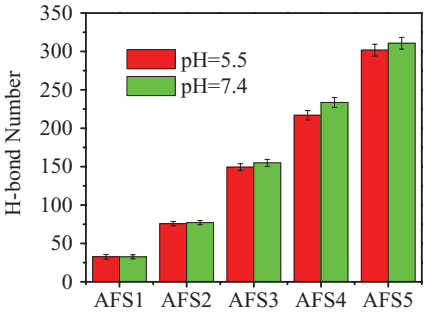

FIG. 2. The average hydrogen bond number of the last 30-ns simulations at pH 5.5 and 7.4 for five hIAPP oligomer species: AFS1, AFS2, AFS3, AFS4, and AFS5.

B. His18 residues

Based on the clues mentioned above, the structural stability of hIAPP protofibrillar oligomer is shown to be highly sensitive to the pH values. As hIAPP monomer contains one His18 residue located at the entrance of the turn (spanning residues 19-24), whose charge state is dependent on pH: protonated at pH 5.5 while deprotonated at pH 7.4. Here, we intend to explore the role of His18 played in the pH-dependent structural dynamics of hIAPP protofibrillar oligomer by doing the structural analysis on His18 residues and residues around them.

1. RMS fluctuations of His18

First, the pH effect on the mobility of His18 residues is examined. Figure 3(a) presents the initial residual structure of His18 within the hIAPP protofibrillar oligomer. Here, we compare the root-mean-square fluctuations (RMSF) of the His18 residues at different pH values. Figures 3(b)–3(f) show the RMSFs of the His18 residues at pH 5.5 (black line) and at pH 7.4 (red line) as a function of His index for AFS1, AFS2, AFS3, AFS4, and AFS5, respectively. Overall, under different pH conditions, the His18 residues display diverse conformational flexibilities. In all simulations His18 residues at low pH exhibit higher RMSF than those at neutral pH, which indicates that the protonated His18 residues at pH 5.5 are more flexible than the deprotonated His18 residues at neutral pH.

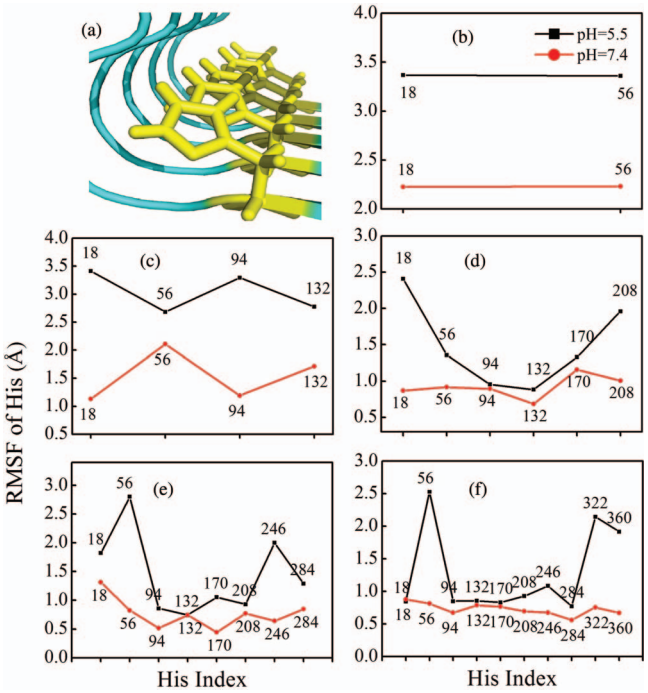

FIG. 3. (a) The structure of five adjacent His residues. RMS fluctuations of the His18 residues at pH 5.5 (black line) and at pH 7.4 (red line) as a function of His index for the systems of (b) AFS1, (c) AFS2, (d) AFS3, (e) AFS4, and (f) AFS5.

As an example shown in Figure 3(c), the four His18 residues of AFS2 at pH 5.5 exhibit large fluctuations between 2.5 Å and 3.5 Å. In contrast, those at pH 7.4 are fluctuating around 1.5 Å. Turning to Figure 3(f), the RMSF values of the His18 residues are about 0.8 Å at pH 7.4. While at pH 5.5 the values are larger, especially the His18 residues located outside, fluctuating over 2.0 Å. As for other oligomer species, the curves of the His18 residues' RMSF values also show a similar trend that the low-pH line is always above the neutral-pH line. Thus, different pH induces a large conformational divergence of the His18 residues, which may be related to the electrostatic interactions. At low pH, the protonated His18 residue introduces one additional charge, leading to the repulsive electrostatic interactions among hIAPP peptides. In addition, the His18 residues located at the outer peptides generally show higher flexibility than those at the inner peptides.

2. Conformational entropy of His18

The conformational entropy provides direct information about the flexibility and stability of a given conformer. Here, we characterize the free energy contribution of conformational entropy (represented by –TS) of the His18 residues in each system as a function of simulation time, displayed in Figures 4(a)–4(e). In an overall view, the entropy contribution becomes basically constant after about 80 ns for all systems at two pH values. Interestingly the equilibrated entropic contributions of all systems at pH 5.5 are lower than those at pH 7.4, especially for the AFS5 (Figure 4(e)), where the entropic component is about –620 kJ/mol at pH 7.4 and –700 kJ/mol at pH 5.5. The lower entropic component under the acidic pH reflects that His18 residues have more conformational states, i.e., are more flexible. Meanwhile, we also analyzed the average conformational entropy difference between two pHs for both the whole system (see x-axis in Figure 4(f)) and for the His18 residues (see y-axis in Figure 4(f)), which is averaged over the last 20-ns simulation trajectories. It is obvious that they are highly correlated in a linear way. The fitting equation is $y = 0.083x - 4.617$, with the correlation coefficient of 0.961. Therefore, the variation of the global conformational state due to pH change is closely correlated to the His18 residues.

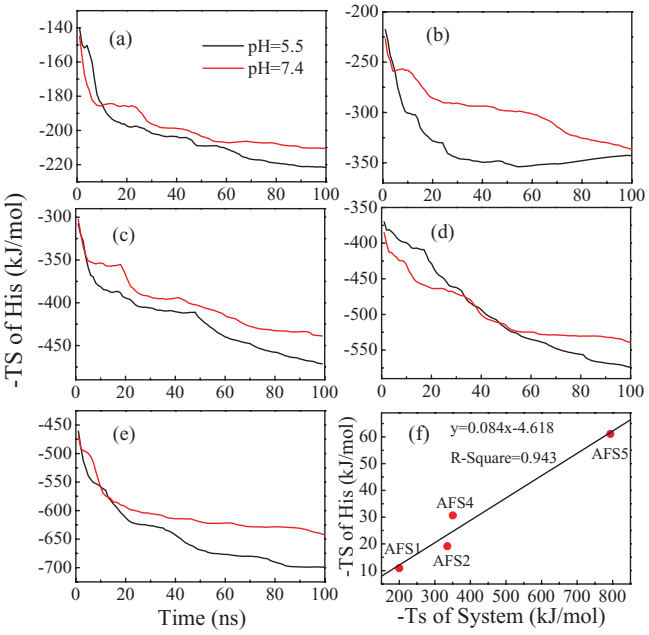

FIG. 4. Time evolution of the free energy contribution of conformational entropy for (a) AFS1, (b) AFS2, (c) AFS3, (d) AFS4, and (e) AFS5. (f) The average conformational entropy difference between two pHs for the whole system (x-axis) and the His structure (y-axis).

C. Local structure around His18

In the following, structural analysis are performed on the local structure around His18 residues. Here, the residues spanning positions 15-21 (totally seven residues) are chosen as the local domain around His18 in each monomer.

1. Secondary structure evolution

To further see the pH effect on the structural details around His18 residues, the secondary structure evolution as a function of simulation time was calculated by DSSP analysis (see Figure 5). The plots on the left side are for simulations at pH 5.5, and those on the right side are for simulations at pH 7.4. The figures from up to down are for residues (spanning positions 15-21 in each monomer) around His18 in AFS1, AFS2, AFS3, AFS4, and AFS5, respectively. As vividly shown in Figure 5, the residues within the local structure under pH 5.5 (on the left side) show more non-β conformations, and those under pH 7.4 (on the right side) mostly retain the β conformations duration the simulations. For example, the secondary structure evolution of AFS4 at pH 5.5 presents more distorted structural characteristics, such as turn, especially for residues around positions 14 (N58) and 28 (N132), 49 (N243). In contrast, the AFS4 at pH 7.4 is almost keeping a perfect β pattern throughout the simulation. This clearly demonstrates that low pH significantly distorts the secondary structure of His18 residues and retards the formation of β conformation. While by observing the DSSP analysis on the whole hIAPP protofibrillar oligomer (data not shown), other residual parts show much less structural changes due to different pH conditions. Therefore, the destabilization effect on the hIAPP oligomers by low pH is mainly concentrated at the vicinity of His18 residues.

2. Hydrogen-bonding network around His18

In the following we calculate the average number of H-bond formed by His18 residues and residues around them (spanning positions 15-21 in each monomer) for AFS1, AFS2, AFS3, AFS4, and AFS5, respectively. The results based on the last 30-ns simulations are shown in Figure 6(a). The green histogram is for pH 5.5, and the red one is for pH 7.4. It is obvious that all the cases at pH 5.5 have fewer H-bond number than those at pH 7.4. Taking AFS5 as an example, when His18 is deprotonated at pH 7.4, it owns nearly 40 H-bonds; while as His18 is protonated at pH 5.5, it has only 29 H-bonds. Fewer H-bond number indicates that the

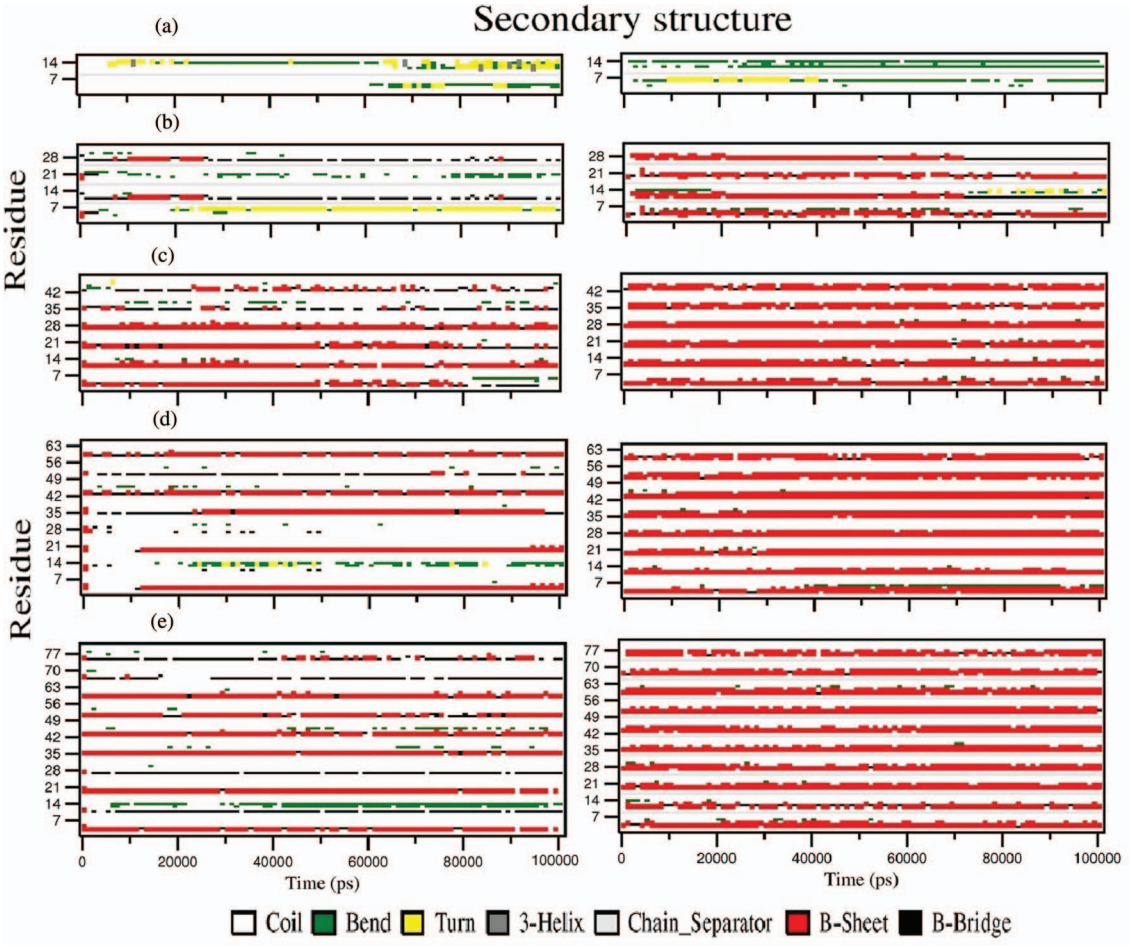

FIG. 5. The secondary structure evolutions of residues around His18 (spanning positions 15-21 in each monomer) as a function of simulation time. The plots on the left side are for simulations at pH 5.5, and those on the right side are for simulations at pH 7.4 for (a) AFS1, (b) AFS2, (c) AFS3, (d) AFS4, and (e) AFS5. The assignment of secondary structures are made with DSSP.

structure is thermodynamically less stable. Thus, the local structure around His18 residue is less stable at pH 5.5 than at pH 7.4.

By means of subtracting the H-bond number at pH 5.5 from the H-bond number at pH 7.4, we further calculate the H-bond number difference due to pH change, for both the whole system and the local structure around His18 residues. The results are shown in Figure 6(b). Interestingly, it is found that the H-bond number difference due to pH change for the whole system is quite close to that for the local structure around His18 residues. This suggests that the ionization state change of His18 by pH triggers the adjustment of the H-bond network within its local structure, which further alters the thermodynamic stability of the whole hIAPP protofibrillar oligomer. Thus, in all, it is the ionization state of His18 that should be responsible for the pH-dependent structural dynamics of hIAPP protofibrillar oligomer, which may practically affect the rate of assembly and morphologies of the fibrillar structures as observed experimentally.[35–37]

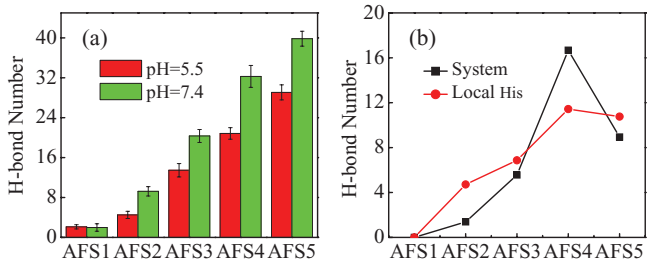

FIG. 6. (a) The average H-bond number of the local structure around His residues (spanning positions 15-21 in each monomer) for the five hIAPP oligomers: AFS1, AFS2, AFS3, AFS4, and AFS5. The green and red histograms are, respectively, for pH 5.5 and pH 7.4. (b) The shifted H-bond number formed by the whole system (the black line) and by the local structure around His residues (the red line) for five systems by subtraction the values at pH 5.5 from those at 7.4.

3. Spacial intimity around His18

To verify it further quantitatively , we also analyze the average center-of-mass (COM) distance and minimum distance between two interchain His18 residues in each system during simulations. Here, the average calculation is performed over both simulation time and multiple His18 pairs. Figure 7(a) shows the COM distance and Figure 7(b) shows the minimum distance between two interchain His18 residues. As clearly shown in the two curves, the values of the distance under pH 7.4 are smaller than those at pH 5.5, which indicates that the local structure around His18 residues is more

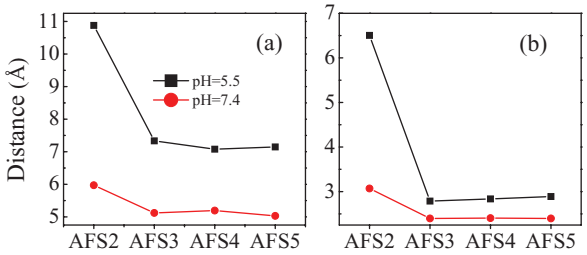

FIG. 7. The average center-of-mass distance (a) and minimum distance (b) between interchain His residues.

intimate under the neutral pH. The COM distance is around 5 Å and 7 Å under pH 7.4 and 5.5, respectively. The larger COM distance under acidic pH indicates that the local structure is pulled apart by the electrostatic repulsive interactions among charged His18 residues. In addition, the minimum distance for each system is about 2–3 Å at pH 7.4. In contrast, the corresponding distances are basically above 3 Å at pH 5.5. Here, the above mentioned 3 Å is only of the minimum distance between two interchain His18 residues. Note that 3 Å between hydrogen and acceptor is a key distance for forming a hydrogen bond. Once beyond this distance, the hydrogen bond would fracture. Thus, consistently, the H-bond number under pH 5.5 is consequently reduced as clearly shown in Figure 6(a).

4. Structural stability

Here, we are interested in the simulated molecular energies to assess the effect of the charge state of His18 on the overall structural stability and local structural stability. Based on the last 30-ns simulation trajectories, the average intra- and inter-molecular energy (electrostatic energy plus van der Waals energy) for the whole structure and for the local structure of AFS1, AFS2, AFS3, AFS4, and AFS5 are calculated and shown in Fig. 8. It is noted that both average molecular energies (Figs. 8(a) and 8(b)) at pH 7.4 is obviously lower than those at pH 5.5. And the energy difference is noticed to be cooperatively increased with the growth of the protofibrillar oligomer. This indicates that the hIAPP protofibrillar oligomer is less stable at pH 5.5. It is in agreement with the above analyses of RMSD, RMSF, and H-bond to qualitatively characterize the structural stability. The agreement supports our conclusion that the structural stability of hIAPP protofibrillar oligomer is disturbed by the repulsive electrostatic interactions among charged His18 residues at pH 5.5.

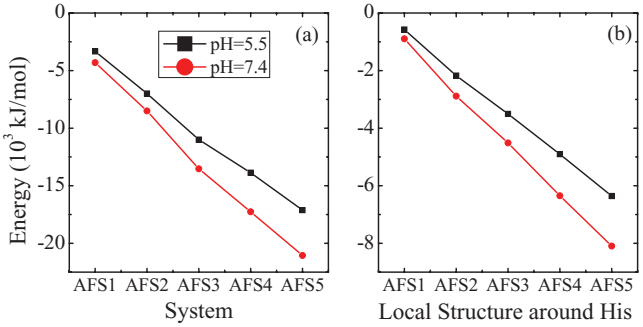

FIG. 8. The average intra- and inter-molecular energy (electrostatic energy plus van der Waals energy) of the last 30-ns simulations at pH 5.5 and 7.4 for (a) the five hIAPP oligomer species: AFS1, AFS2, AFS3, AFS4, and AFS5; (b) the local structure around His residues (spanning positions 15-21 in each monomer) for the five hIAPP oligomers.

D. Folding trial by a coarse-grained model

Finally, in order to test the effect of ionization state of His18 on hIAPP aggregation, a structure-based coarse-grained model is applied to calculate the dimerization rate of two full-length hIAPP monomers with the His18 residues in non-charged (Fig. 9(a)) or charged states (Fig. 9(b)). In our simulations, the initial structure of hIAPP dimer is obtained from the unfolded ensemble after a long-time high-temperature (500 K) unfolding simulation, of which two monomers are in random coil conformations (see Fig. 9). The simulated dimerization rate at 300 K with the His18 residues in non-charged state is $17.4 \pm 2.6\ \mu s^{-1}$. While the simulated dimerization rate with the His18 residues in charged state is $7.8 \pm 1.9\ \mu s^{-1}$. Thus, the repulsive electrostatic interactions among charged His18 residues slow down the dimerization process of hIAPP by around twofold. Figure 8 shows the two representative folding trajectories at 300 K: time evolution of the fraction of native contacts (Q). With the two His18 residues in non-charged states (to mimic the neutral pH condition), the dimerization process is finished at the simulation time of 50 ns (Figure 8(a)). And a transient (34 ns-47 ns) intermediate state is visited. The whole dimerization process is of an approximate two-state behavior: from unfolded state (random coil) to folded state (dimer). While with the two His18 residues in positively charged states (to mimic the acidic pH condition), the dimer is formed until 400 ns owing to the retarding effect by the repulsive electrostatic interactions among charged His18 residues. The folding rate is significantly slower than the former case. The dimerization dynamics is significantly slowed down due to the electrostatic repulsive interactions among two charged His18 residues. Within the window of 300-ns simulation time (see Figure 8(b)), a partially folded intermediate state clearly exists (lasting

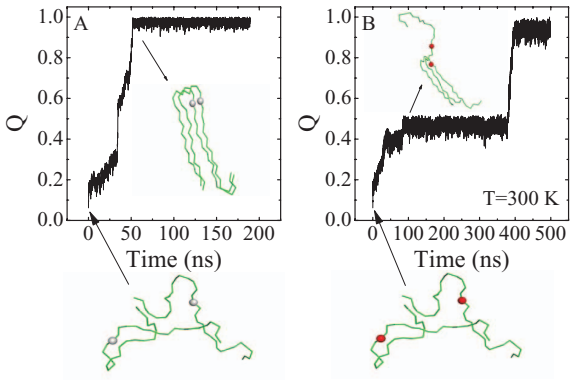

FIG. 9. Time evolution of the fraction of native contacts Q. $Q = 1$ means the hIAPP dimer is completely formed, while $Q = 0$ indicates the dimer is completely unfolded. Dimerization trajectory of hIAPP at 300 K based on a coarse-grained model for (a) neutral His and (b) charged His. The gray and red spheres denote two neutral and charged His18 residues, respectively.

350 ns) during the dimerization process. Thus, the ionization state of His18 due to pH conditions does affect the aggregation dynamics of hIAPP.

IV. CONCLUSIONS

Human IAPP peptide is largely in soluble form at acid pH, but in extracellular neutral-pH compartment easily accumulates to amyloid fibrils. And the morphologies of the fibrillar structures and the aggregation rate are highly sensitive to the pH values.[35–37] Employing constant pH molecular dynamics simulations of two Aβ peptide segments, Aβ(1–28) and Aβ(10–42), Khandogin and Brooks III found that the folding landscape of the peptides is strongly modulated by pH.[39] A multiscale simulation study by Derreumaux and De Simone showed that the protonation of His sidechains led to an enhanced conformational heterogeneity of the NHVTLSQ heptamers at pH 4.[55] A very recent experiment by Khemtemourian *et al*.[35] found that acidic pH acts as an inhibitor of the fibril formation of hIAPP. In this article, we intend to investigate the underlying potential mechanism of the pH effects on fibrillogenesis of hIAPP. All-atom MD simulations of several hIAPP protofibrillar oligomers were performed at different pH values under standard AMBER99SB force fields. It is notable that the force field-dependent peptide/protein conformational bias is arousing more and more attentions.[56,57] It is found that GROMOS96 and AMBER99 force fields are biased toward amyloid-like and α-helical structures, respectively. In contrast, the OPLS force field provides a wide conformational distribution.[56] Very recently, the ff99sb-ildn-phi and ff99sb-ildn-NMR force fields are shown to achieve high accuracy in calculating the experimental observables.[57] Here, the simulations under AMBER99SB just give comparative results due to different pH conditions. Simulation results show that the dynamical stability of hIAPP protofibrillar oligomers is significantly influenced by pH. An acidic pH of 5.5 destabilizes the assembly structure of oligomers, while the structure is more stable under a neutral pH of 7.4. Monomeric hIAPP contains one His18 residue located at the entrance of the turn (spanning residues 19–24), whose charge state is dependent on pH: protonated at pH 5.5 while deprotonated at pH 7.4. Simulation results reveal that low pH significantly distorts the secondary structure of His18 residues, which consequently destroys the H-bond network of the local structure around His18 in the hIAPP oligomers. As a result, the assembly structure becomes thermodynamically less stable. Thus, protonated His18 acts as an assembly blocker that retards the fibrillization of hIAPP. Interestingly, it is further found that the H-bond number difference due to pH change for the whole system is quite close to that for the local structure around His18 residues. This suggests that the ionization state change of His18 by pH triggers the adjustment of the H-bond network within its local structure, which further alters the thermodynamic stability of the whole hIAPP protofibrillar oligomer. In addition, a complementary coarse-grained simulation clearly shows that the repulsive electrostatic interactions among charged His18 residues slow down the dimerization process of hIAPP by 2-fold. Thus, in all, it is the ionization state of His18 that should be responsible for the pH-dependent structural dynamics of hIAPP protofibrillar oligomer, which may practically affect the rate of assembly and morphologies of the fibrillar structures as observed experimentally.[35–37] Certainly, since human IAPP does not form amyloid in nondiabetic individuals, factors other than these pH changes must also contribute to amyloid formation.[58,59]

ACKNOWLEDGMENTS

We thank the National Natural Science Foundation of China (NNSFC) (Grant Nos. 21003048, 10974054, 20933002, and 11204083). W.X.X. is grateful to Research Fund for the Doctoral Program of Higher Education of China (20120076120033) and Shanghai PuJiang program (12PJ1403000) for financial support. We also thank the supercomputer center at ECNU for computer time.

[1] F. Chiti and C. M. Dobson, Annu. Rev. Biochem. **75**, 333 (2006).
[2] D. J. Selkoe, Nature (London) **428**, 445 (2004).
[3] J. D. Sipe, Amyloidosis. Crit Rev Cl Lab Sci. **31**, 325 (1994).
[4] Y. C. Kudva, C. Mueske, P. C. Butler, and N. L. Eberhardt, Biochemical Journal **331**, 809 (1998).
[5] R. A. DeFronzo, Diabetes **37**, 667 (1988).
[6] C. Rocken, R. P. Linke, and W. Saeger, Virchows Arch. A: Pathol. Anat. Histopathol. **421**, 339 (1992).
[7] H. M. Schneider, S. Storkel, and W. Will, Dtsch. Med. Wochenschr. **105**, 1143 (1980).
[8] S. E. Kahn, S. Andrikopoulos, and C. Verchere, Diabetes **48**, 241 (1999).
[9] A. Clark, C. A. Wells, I. D. Buley, J. K. Cruickshank, R. I. Vanhegan, D. R. Matthews, G. J. Cooper, R. R. Holman, and R. C. Turner, Diabetes Res. **9**, 151 (1988).
[10] A. Lorenzo, B. Razzaboni, G. C. Weir, and B. A. Yankner, Nature (London) **368**, 756 (1994).
[11] D. Schubert, C. Behl, R. Lesley, A. Brack, R. Dargusch, Y. Sagara, and H. Kimura, Proc. Natl. Acad. Sci. U.S.A. **92**, 1989 (1995).
[12] J. W. M. Hoppener, B. Ahren, and C. J. Lips, N. Engl. J. Med. **343**, 411 (2000).
[13] P. Westermark, C. Wernstedt, E. Wilander, D. W. Hayden, T. D. O'Brien, and K. H. Johnson, Proc. Natl. Acad. Sci. U.S.A. **84**, 3881 (1987).
[14] G. J. Cooper, A. C. Willis, A. Clark, R. C. Turner, R. B. Sim, and K. B. Reid, Proc. Natl. Acad. Sci. U.S.A. **84**, 8628 (1987).
[15] A. V. Kajava, U. Aebi, and A. C. Steven, J. Mol. Biol. **348**, 247 (2005).
[16] S. Luca, W. M. Yau, R. Leapman, and R. Tycko, Biochemistry **46**, 13505 (2007).
[17] J.-J. W. Wiltzius, S. A. Sievers, M. R. Sawaya, D. Cascio, D. Popov, C. Riekel, and D. Eisenberg, Protein Sci. **17**, 1467 (2008).
[18] C. Goldsbury, P. Frey, V. Olivieri, U. Aebi, and S. A. Muller, J. Mol. Biol. **352**, 282 (2005).
[19] J. D. Green, C. Goldsbury, J. Kistler, G. J. S. Cooper, and U. Aebi, J. Biol. Chem. **279**, 12206 (2004).
[20] W. X. Xu, J. Ping, W. F. Li, and Y. G. Mu, J. Chem. Phys. **130**, 164709 (2009).
[21] A. T. Petkova, R. D. Leapman, Z. H. Guo, W. M. Yau, M. P. Mattson, and R. Tycko, Science **307**, 262 (2005).
[22] M. Gregori, V. Cassina, D. Brogioli, D. Salerno, L. De Kimpe, W. Scheper, M. Masserini, and F. Mantegazza, Eur. Biophys. J. **39**, 1613 (2010).
[23] J. Dong, J. M. Canfield, A. K. Mehta, J. E. Shokes, B. Tian, W. S. Childers, J. A. Simmons, Z. Mao, R. A. Scott, K. Warncke, and D. G. Lynn, Proc. Natl. Acad. Sci. U.S.A. **104**, 13313 (2007).
[24] A. Morriss-Andrews, G. Bellesia, and J. E. Shea, J. Chem. Phys. **135**, 085102 (2011).
[25] Z. M. Fu, Y. Luo, P. Derreumaux, and G. H. Wei, Biophys. J. **97**, 1795 (2009).
[26] P. Jiang, W. Li, J. E. Shea, and Y. G. Mu, Biophys. J. **100**, 1550 (2011).
[27] A. Huet and P. Derreumaux, Biophys. J. **91**, 3829 (2006).
[28] R. Tycko, K. L. Sciarretta, J. Orgel, and S. C. Meredith, Biochemistry **48**, 6072 (2009).
[29] W. H. Xi, W. F. Li, and W. Wang, J. Phys. Chem. B **116**, 7398 (2012).

[30]P. Jiang, L. Wei, K. Pervushin, and Y. G. Mu, J. Phys. Chem. B **114**, 10176 (2010).
[31]J. C. Hutton, Diabetologia **32**, 271 (1989).
[32]S. E. Kahn, D. A. D'Alessio, M. W. Schwartz, W. Y. Fujimoto, J. W. Ensinck, G. J. Taborsky, Jr., and D. Porte, Jr., Diabetes **39**, 634 (1990).
[33]T. Sanke, T. Hanabusa, Y. Nakano, C. Oki, K. Okai, S. Nishimura, M. Kondo, and K. Nanjo, Diabetologia **34**, 129 (1991).
[34]P. C. Butler, J. Chou, W. B. Carter, Y. N. Wang, B. H. Bu, D. Chang, J. K. Chang, and R. A. Rizza, Diabetes **39**, 752 (1990).
[35]L. Khemtemourian, E. Domenech, J. P. F. Doux, M. C. Koorengevel, and J. A. Killian, J. Am. Chem. Soc. **133**, 15598 (2011).
[36]A. Abedini and D. P. Raleigh, Biochemistry **44**, 16284 (2005).
[37]E. Jaikaran, C. E. Higham, L. C. Serpell, J. Zurdo, M. Gross, A. Clark, and P. E. Fraser, J. Mol. Biol. **308**, 515 (2001).
[38]V. Hornak, R. Abel, A. Okur, B. Strockbine, A. Roitberg, and C. Simmerling, Proteins **65**, 712 (2006).
[39]J. Khandogin and C. L. Brooks III, Proc. Natl. Acad. Sci. U.S.A. **104**, 16880 (2007).
[40]W. X. Xu, C. Zhang, P. Derreumaux, A. Graslund, L. Morozova-Roche, and Y. G. Mu, PLoS ONE **6**, e24329 (2011).
[41]W. X. Xu, C. Zhang, L. Morozova-Roche, J. Z. H. Zhang, and Y. G. Mu, J. Phys. Chem. B **117**(28), 8392–8399 (2013).
[42]H. J. C. Berendsen, D. van der Spoel, and R. van Drunen, Comput. Phys. Commun. **91**, 43 (1995).
[43]C. Duan, Y. Wu, S. Chowdhury, M. C. Lee, G. M. Xiong, W. Zhang, R. Yang, P. Cieplak, R. Luo, T. Lee, J. Caldwell, J. M. Wang, and P. Kollman, J. Comput. Chem. **24**, 1999 (2003).
[44]B. Hess, H. Bekker, H. J. C. Berendsen, and J. G. E. M. Fraaije, J. Comput. Chem. **18**, 1463 (1997).
[45]M. Patra, M. Karttunen, M. T. Hyvonen, E. Falck, P. Lindqvist, and I. Vattulainen, Biophys J. **84**, 3636 (2003).
[46]T. Darden, D. York, and L. Pedersen, J. Chem. Phys. **98**, 10089 (1993).
[47]C. Clementi, H. Nymeyer, and J. N. Onuchic, J. Mol. Biol. **298**, 937 (2000).
[48]W. Wang, W. X. Xu, Y. Levy, E. Trizacc, and P. G. Wolynes, Proc. Natl. Acad. Sci. U.S.A. **106**, 5517 (2009).
[49]T. Frembgen-Kesner and A. H. Elcock, J. Chem. Theory Comput. **5**, 242 (2009).
[50]D. L. Pincus, S. S. Cho, C. Hyeon, D. Thirumalai, and P. M. Conn, "Minimal models for proteins and RNA: From folding to function," in *Molecular Biology of Protein Folding, Part B* (Academic Press, 2008), Vol. 84, Chap. VI, pp. 203–250.
[51]W. Kabsch and C. Sander, Biopolymers **22**, 2577 (1983).
[52]B. Viskolcz, S. N. Fejer, S. J. K. Jensen, A. Perczel, and I. G. Csizmadia, Chem. Phys. Lett. **450**, 123 (2007).
[53]B. Viskolcz, I. G. Csizmadia, S. J. K. Jensen, and A. Perczel, Chem. Phys. Lett. **501**, 30 (2010).
[54]I. Andricioaei and M. Karplus, J. Chem. Phys. **115**, 6289 (2001).
[55]A. De Simone and P. Derreumaux, J. Chem. Phys. **132**, 165103 (2010).
[56]P. H. Nguyen, M. S. Li, and P. Derreumaux, Phys. Chem. Chem. Phys. **13**, 9778 (2011).
[57]K. A. Beauchamp, Y. S. Lin, R. Das, and V. S. Pande, J. Chem. Theory. Comput. **8**, 1409 (2012).
[58]E. Jaikaran, M. R. Nilsson, and A. Clark, Biochem. J. **377**, 709 (2004).
[59]J. L. Larson and A. D. Miranker, J. Mol. Biol. **335**, 221 (2004).